

Document downloaded from:

<http://hdl.handle.net/10251/141527>

This paper must be cited as:

Pérez Arjona, I.; Godinho, L.; Espinosa Roselló, V. (2018). Numerical simulation of target strength measurements from near to far field of fish using the method of fundamental solutions. *Acta Acustica united with Acustica*. 104(1):25-38.  
<https://doi.org/10.3813/AAA.919142>



The final publication is available at

<https://doi.org/10.3813/AAA.919142>

Copyright S. Hirzel Verlag

Additional Information

Numerical simulation of target strength measurements  
from near to far field of fish using the method of  
fundamental solutions

5

Isabel Pérez-Arjona

Institut d'Investigació per a a Gestió Integrada de Zones Costaneres,  
Universitat Politècnica de València, 46730 Grau de Gandia, Spain

[iparjona@upv.es](mailto:iparjona@upv.es)

10

Luís M. C. Godinho

ISISE, Departamento de Engenharia Civil – FCTUC, Universidade de  
Coimbra,

3030 - 788 Coimbra, Portugal

[lgodinho@dec.uc.pt](mailto:lgodinho@dec.uc.pt)

15

Víctor Espinosa

Institut d'Investigació per a a Gestió Integrada de Zones Costaneres,  
Universitat Politècnica de València, 46730 Grau de Gandia, Spain

20

[vespinos@upv.es](mailto:vespinos@upv.es)

August, 2016

## Summary

We propose the application of a numerical model based on the Method of Fundamental  
 5 Solutions to the estimation of the target strength (TS) of single fish, a crucial parameter for  
 evaluating fish abundance when using active acoustical techniques. We consider a realistic  
 beam and the influence of the evolution of the scattered field with distance maintaining the  
 target in the far field of the ultrasonic transducer. The cases of a fluid sphere and a prolate  
 spheroid model for the swimbladder are used to verify the application of MFS against other  
 10 analytical and numerical methods. Additionally, a model considering only the swimbladder and  
 the fishbone is presented to evaluate the differences between dorsal and ventral aspect  
 measurements, and to understand previous experimental works performed with Atlantic salmon  
 (*Salmo salar*) in floating cages.

15 PACS no 43.30.+m, 43.30.Gv, 43.30.Sf, 44.05.+e

## 1. Introduction

The target strength (TS) of single fish, a  
 20 parameter related to the acoustical  
 reflectivity, is a fundamental input  
 value for fish abundance estimations  
 when using active acoustical techniques.  
 Such techniques assume that the total  
 25 integrated echo energy returned from  
 randomly distributed targets inside the  
 acoustic beam is proportional to the  
 quantity of those targets and to the echo  
 intensity returned by an average

30 scatterer [1, section 2.5.6]. Therefore  
 the characterisation of the TS of  
 different species, and its variability  
 under different changing factors like  
 fish orientation, depth and physiological  
 35 factors, have been an important part of  
 the research developed in fisheries  
 acoustics since the early 80's [1, section  
 6.3]. Three alternative or  
 complementary methods are used for  
 40 TS estimations: (i) *in situ* measurements  
 of fish in the wild, (ii) *ex situ* techniques  
 by measuring constrained fish (dead or  
 alive), and (iii) theoretical modelling of

the acoustic field backscattered by the  
45 fish's main anatomical structures [2].

We are interested in the experimental  
situation that is common to different  
scenarios and applications of fisheries  
acoustics: very shallow waters (like in  
50 rivers and ponds), aquaculture floating  
cages or biomass characterisation close  
to fishing aggregating devices (FADs).  
They have in common that the TS  
measurements are usually conducted at  
55 close distances of fish, and some errors  
associated with the near range are  
expected. These errors include: the TS  
dependence with distance due to  
extension of the near field of the  
60 transducer and also of fish as scatterers  
[1, section 2.4.1]; the point-source  
principle violation, that affects the  
accuracy of the applied time-varying  
gain or TVG [3-78]; the extended size  
65 of fish, which also produces an  
indetermination in the position inside  
the beam measured by split-beam  
echosounders and therefore in the  
directivity gain compensation [10-123];  
70 and even the partial insonification of  
fish [13].

Assuming that the near field of the  
transducer is known from the equipment

specifications, and that the related  
75 minimal operational distance is  
respected, our interest is focused on the  
more elusive answer about the far-  
enough distance to achieve the far field  
condition from the fish, and to minimize  
80 the above referred near distance effects  
associated to its size when compared to  
the beam volume. Some experimental  
results found in the literature suggested  
that fish size (or the relative close  
85 distance to the fish) could have  
conditioned their TS measurements [13-  
15], whilst other minimize its influence  
[16].

TS measurements on caged salmon  
90 (*Salmo salar*) have been addressed to  
monitor fish growth and total biomass  
evolution inside floating cages by  
Knudsen *et al.* [13]. The results of such  
work have shown a good correlation of  
95 TS versus fish length (20-78 cm) at high  
frequencies (120 and 200 kHz) with  
uni-modal distributions of TS for each  
class size from ventral aspect; in the  
dorsal case, the distributions were  
100 shown to be bi- or tri-modal (mainly for  
the smaller fishes) and a much poorer  
correlation of TS with fish length was  
found. TS dependence with distance (6  
to 18 m) was reported as not relevant

105 for both observed fish aspects.

In the case of tuna, measurements in cages can provide TS values for new techniques of biomass estimation in the wild [17], or to improve size and species discrimination in fish aggregating devices (FADs) equipped with quantitative echosounders [18]. Preliminary works with caged bluefin tuna (*Thunnus thynnus*, fork length of 115 130-210 cm) showed a similar tendency to that of salmon, with ventral aspect being the only one suitable for size monitoring in spite of partial insonification [14]. Dorsal 120 measurements of juvenile yellowfin (*Thunnus albacares*) were performed in [15] both *in situ* (around a FAD) and *ex situ* (in a tank); obtaining for the last set of data a poor linear correlation 125 coefficient ( $R^2=0.42$ ) between TS and optically measured fork length (25–80 cm tuna at a distance between 2.6 and 3.4 m).

Nevertheless, a recent *ex situ* 130 experiment from lateral aspect with fresh water species (Andalusian barbel, *Luciobarbus sclateri*, and carp, *Cyprinus carpio*, between 325 and 525 mm of length) did not seem to show TS

135 dependence with distance (6 to 12 m) [16].

At this point we consider as necessary to develop appropriate simulations to investigate numerically the possible 140 effects of the near field of fish, as a function of aspect, combined with the interplay between fish size and beam dimensions and transducer directivity in its far field. As a first step, we must 145 chose a simulation method with the possibility of evaluating the measured TS for an increasing distance of fish to the transducer.

A lot of acoustic scattering models to 150 predict acoustic backscatter by fish and zooplankton have been developed since the 1960s [19] and were recently summarised and compared [20, 21]. Particularly, for the case of fish with 155 gas-filled swimbladder: the *T*-matrix method [22], scattering models based on cylinders [23-25], the Kirchhoff-Approximation (KA) [26] and Kirchhoff-ray-mode model (KRM) [27], 160 the analytical model based in a modal expansion of a prolate-spheroid [6], the Fourier mode matching method [28] and the numerical solution of the Helmholtz equation using either the

165 finite element method (FEM) [29] or  
the boundary element method (BEM)  
[30].

A reasonable agreement between *in situ*  
and *ex situ* measurements and  
170 simulations has been reached mainly  
with Kirchoff approaches [31-34],  
with differences between modelled and  
measured TS depending on the tilt angle  
distributions [32,35-37].

175 The main similarity in all cited efforts is  
the evaluation of TS in the far field; in  
fact only FEM and BEM can calculate  
TS at a desired finite distance whilst the  
rest of cited methods have assumed in  
180 different ways the far field condition.  
However, this capability has not been  
exploited due to the high, or even  
unaffordable, computational cost (even  
higher with FEM, as a volume mesh  
185 method for field propagation).

In recent decades, a new class of  
numerical methods has emerged,  
namely meshless methods, which have  
been in progressive development  
190 aiming mostly at a reduction of  
computational costs and of the effort  
involved in the discretization of the  
problem geometry. Within this class,  
the Method of Fundamental Solution

195 (MFS) has merited attention for  
acoustic problems, since, as happens  
with the BEM, it makes use of  
fundamental solutions that directly  
account for infinite or semi-infinite  
200 spaces. However, its mathematical  
formulation and implementation are  
much simpler, since it is based on a  
collocation approach without requiring  
any numerical or analytical integration.  
205 In fact, the method is simply based on a  
linear superposition of fundamental  
solutions to approximate the solution of  
the problem, assuming sources located  
outside of the computational domain to  
210 avoid singularities in the solution. There  
is extensive literature regarding the  
MFS and its application to acoustic  
scattering and/or radiation problems,  
such as the early works of Fairweather  
215 *et al.* [38]. More recently, the method  
has been successfully applied to model  
acoustic problems in the fields of room  
acoustics [39], acoustic radiation  
problems [40] and underwater acoustics  
220 [41]. Detailed numerical studies  
regarding the stability and accuracy of  
the MFS have also been published [42],  
demonstrating that the simple  
mathematical formulation of the MFS  
225 and its high accuracy can result in

significant computational resource savings if large problems are considered. The above mentioned studies have also evidenced that the MFS can have some limitations when applied to complex geometries with sharp edges, for which the simple setup of the method may not be able to reproduce the acoustic field accurately. However, the application of the MFS to smooth geometries, both in 2D and 3D, seems to be advantageous and to allow some important computational gains.

In this context, we propose the application of the MFS for the solution of the Helmholtz equation at arbitrary distances of an idealized fish model. In the following sections the method will be described, verified through the calculation of the TS of different cases of fluid spheres and a gas-filled prolate-spheroid and the comparison against other methods [20], and finally applied to investigate its potential in a case study, with the fish modelled by its swimbladder and spine bone, using its predictions to interpret the experimental results of Knudsen *et al.* [13].

## 2. Material and methods

### 2.1 Mathematical formulation of MFS

#### 2.1.1. Governing equations

The propagation of sound within a homogeneous acoustic space can be mathematically represented in the frequency domain by the Helmholtz differential equation,

$$\nabla^2 p + k^2 p = 0 \quad (1)$$

where  $\nabla^2 = \frac{\partial^2}{\partial x^2} + \frac{\partial^2}{\partial y^2} + \frac{\partial^2}{\partial z^2}$  in the case of a 3D problem;  $p$  [Pa] is the acoustic pressure,  $k = \omega/c$  the wave number,  $\omega = 2\pi f$  the angular frequency,  $f$  [Hz] the frequency and  $c$  [m/s] the sound propagation velocity within the acoustic medium.

For the 3D case, assuming a point source placed within the propagation domain, at point  $\mathbf{x}_0$  with coordinates  $(x_0, y_0, z_0)$  [m], it is possible to establish fundamental solutions  $G$ , for the sound pressure, and  $H$ , for the particle velocity [m/s], at a point  $\mathbf{x}$  with coordinates  $(x, y, z)$  [m], which can be written respectively as:

$$G^{3D}(\mathbf{x}, \mathbf{x}_0, k) = \frac{e^{-ikr}}{r}, \quad (2)$$

$$H^{3D}(\mathbf{x}, \mathbf{x}_0, k, \bar{\mathbf{n}}) = \frac{1}{-i\rho\omega} \frac{(-ikr-1)e^{-ikr}}{r^2} \frac{\partial r}{\partial \bar{\mathbf{n}}}. \quad (3)$$

In these equations,  $r$  [m] corresponds to the distance between the source point and the domain point, given;  $\bar{\mathbf{n}}$  represents the direction along which the particle velocity is calculated and  $\rho$  [kg/m<sup>3</sup>] the medium density.

### 2.1.2. MFS Formulation

While fish have a number of anatomical features that can affect TS, we chose to focus on flesh and vertebrae, because all fish have these throughout their live, and some have a gas-filled swimbladder, which is known to dominate TS in the Rayleigh, resonant, and into the geometric scattering regions. It is important to understand that under this consideration the most significant contribution of the acoustic scattering from fish at the frequency range of the commercial echosounders is due to the swimbladder (when present) [26] and, eventually, from the bony structures (skull and spine), since

these two internal elements are the ones with more important contrast with respect to the water. As for the fish flesh, its properties are, usually, closer to those of the host medium (water) than the other fish structures [43]. Even though, a more general numerical model should simulate as accurately as possible the presence of these three components, accounting for their internal properties like in Figure 1.a). Since the swimbladder is usually gas-filled, the contrast with respect to the surrounding water is quite strong, and so its boundary can be basically seen as a pressure release interface. As for the flesh, skull and spine, its properties are much closer to those of the water than for the swimbladder, and their presence must be simulated as a heterogeneity with its own properties. The complex geometry of the skull and spine, together with their elastic properties, condition severely the feasibility of numerical simulations. Even more, the contribution of shear waves has been reported to be not relevant for the backscattering of backbone in previous works [44], even more in the case of low and medium frequencies (<150 kHz). Therefore in this work we will



consider only the propagation of longitudinal waves along the fish spine.

340 In a first approach and in order to evaluate the main contributions to the scattering properties of fish, we propose a simplified fish model that includes:

- The swimbladder, simulated as a volume with pressure release boundary conditions at its surface;
- The spine, modelled as a fluid filled inclusion, with distinct properties from the host medium.
- The flesh, modelled as a fluid surrounding the spine and the swimbladder with slightly different properties from the water

We will particularize this three component model in the following to verify the validity of application of MFS in different cases,

To formulate the MFS for the analysis of acoustic scattering by a system, it is first necessary to understand that the basic principle of the MFS is that the sound field in a homogeneous region can be simulated by the linear

superposition of the effects of a number of virtual sources, each one with its own amplitude. So, to define the formulation of this problem, let us first consider five sets of virtual sources located: the first and second on the inner and outer sides of the flesh-water interface, respectively, each with NS1 sources; the third and fourth on the inner and outer sides of the spine's surface, each with NS2 sources; the fifth within the swim bladder, with NS3 sources.

The first set is responsible for the simulation of the sound field in the host water medium (here designated as  $\Omega_1$ ), and allows sound field to be written as

$$p(\mathbf{x}, k)_{\Omega_1} = \sum_{j=1}^{NS1} P_j G^{3D}(\mathbf{x}, \mathbf{x}_{1,j}, k_1) + p_{inc}(\mathbf{x}, \mathbf{x}_{source}, k_1) \text{ for } \mathbf{x} \text{ in } \Omega_1 \quad (4)$$

Using the second, third and fifth sets of virtual sources, the sound field within the flesh (medium  $\Omega_2$ ) can be computed as:

$$p(\mathbf{x}, k)_{\Omega_2} = \sum_{j=1}^{NS1} Q_j G^{3D}(\mathbf{x}, \mathbf{x}_{2,j}, k_2) + \sum_{j=1}^{NS2} R_j G^{3D}(\mathbf{x}, \mathbf{x}_{3,j}, k_2) + \sum_{j=1}^{NS3} T_j G^{3D}(\mathbf{x}, \mathbf{x}_{5,j}, k_2) \text{ for } \mathbf{x} \text{ in } \Omega_2 \quad (5)$$

Finally, using the fourth set of sources  
 390 located around the spine, the sound field  
 within the spine can be calculated as

$$p(\mathbf{x}, k_3)_{\Omega_3} = \sum_{j=1}^{NS2} S_j G^{3D}(\mathbf{x}, \mathbf{x}_{4,j}, k_3) \quad (6)$$

for  $\mathbf{x}$  in  $\Omega_3$

In Equations (4), (5) and (6),  $P_j$ ,  $Q_j$ ,  
 $R_j$ ,  $S_j$  and  $T_j$  are unknown  
 395 amplitudes of the virtual sources,  
 $p_{inc}(\mathbf{x}, \mathbf{x}_{source}, k)$  represents the incident  
 field generated by a source located at  
 $\mathbf{x}_{source}$ , and  $k_1$ ,  $k_2$  and  $k_3$  represent the  
 wavenumber in the host medium  
 400 (water), in the flesh and in the spine,  
 respectively. To determine the relevant  
 amplitudes, a system of equations must  
 be established by imposing the  
 necessary interface and boundary  
 405 conditions. For that purpose, it is  
 necessary to consider:

- continuity of pressure and of  
 normal particle velocity in the  
 interface between the host water  
 410 medium and the flesh ( $\Gamma_1$ );
- continuity of pressure and of  
 normal particle velocity in the  
 interface between the flesh and  
 the spine ( $\Gamma_2$ );

- null pressure along the  
 boundary surface of the  
 swimbladder ( $\Gamma_3$ ).

Mathematically, these conditions can be  
 written as:

$$420 p(\mathbf{x}, k_1)_{\Omega_1} = p(\mathbf{x}, k_2)_{\Omega_2}, \mathbf{x} \in \Gamma_1 \quad (7)$$

$$v(\mathbf{x}, k_1, \vec{n})_{\Omega_1} = v(\mathbf{x}, k_2, \vec{n})_{\Omega_2}, \mathbf{x} \in \Gamma_1 \quad (8)$$

$$p(\mathbf{x}, k_2)_{\Omega_2} = p(\mathbf{x}, k_3)_{\Omega_3}, \mathbf{x} \in \Gamma_2 \quad (9)$$

$$v(\mathbf{x}, k_2, \vec{n})_{\Omega_2} = v(\mathbf{x}, k_3, \vec{n})_{\Omega_3}, \mathbf{x} \in \Gamma_2 \quad (10)$$

$$p(\mathbf{x}, k_2)_{\Omega_2} = 0, \mathbf{x} \in \Gamma_3 \quad (11)$$

425 To completely establish the formulation  
 of the method, a number of collocation  
 points must be considered throughout  
 the surfaces of the spine, of the  
 swimbladder and of the flesh. Figure  
 430 1.b) illustrates the typical configuration  
 and the location of these points, also  
 identifying the three acoustic media  $\Omega_1$   
 (water),  $\Omega_2$  (flesh) and  $\Omega_3$  (spine), as  
 well as their boundaries  $\Gamma_1$  (interface  
 435 between flesh and water),  $\Gamma_2$  (interface  
 between the flesh and the spine) and  
 $\Gamma_3$  (boundary of the swim bladder).

Imposing these boundary conditions at  
 those discrete points homogeneously  
 440 distributed throughout the three surfaces

(points  $\bar{\mathbf{x}}_{i,\Gamma_1}$ ,  $\bar{\mathbf{x}}_{i,\Gamma_2}$  and  $\bar{\mathbf{x}}_{i,\Gamma_3}$ ), an equation system with (2xNS1+2xNS2+NS3) equations on (2xNS1+2xNS2+NS3) unknowns can be written. Equation (12) gives a generic representation of this system of equations.

$$\mathbf{Ax} = \mathbf{B} \Leftrightarrow \begin{bmatrix} \mathbf{G}_{\Gamma_1,1,\Omega_1} & -\mathbf{G}_{\Gamma_1,2,\Omega_2} & -\mathbf{G}_{\Gamma_1,3,\Omega_2} & \cdots \\ \mathbf{H}_{\Gamma_1,1,\Omega_1} & -\mathbf{H}_{\Gamma_1,2,\Omega_2} & -\mathbf{H}_{\Gamma_1,3,\Omega_2} & \cdots \\ 0 & \mathbf{G}_{\Gamma_2,2,\Omega_2} & \mathbf{G}_{\Gamma_2,3,\Omega_2} & \cdots \\ 0 & \mathbf{H}_{\Gamma_2,2,\Omega_2} & \mathbf{H}_{\Gamma_2,3,\Omega_2} & \cdots \\ 0 & \mathbf{G}_{\Gamma_3,2,\Omega_2} & \mathbf{G}_{\Gamma_3,3,\Omega_2} & \cdots \\ \cdots & 0 & -\mathbf{G}_{\Gamma_1,5,\Omega_2} & \\ \cdots & 0 & -\mathbf{H}_{\Gamma_1,5,\Omega_2} & \\ \cdots & -\mathbf{G}_{\Gamma_2,4,\Omega_3} & \mathbf{G}_{\Gamma_2,5,\Omega_2} & \\ \cdots & -\mathbf{H}_{\Gamma_2,4,\Omega_3} & \mathbf{H}_{\Gamma_2,5,\Omega_2} & \\ \cdots & 0 & \mathbf{G}_{\Gamma_3,5,\Omega_2} & \end{bmatrix} \begin{bmatrix} \mathbf{P} \\ \mathbf{Q} \\ \mathbf{R} \\ \mathbf{S} \\ \mathbf{T} \end{bmatrix} = \begin{bmatrix} -\mathbf{p}_{inc,\Gamma_1} \\ -\mathbf{v}_{inc,\Gamma_1} \\ 0 \\ 0 \\ 0 \end{bmatrix} \quad (12)$$

$\mathbf{P}$ ,  $\mathbf{Q}$ ,  $\mathbf{R}$ ,  $\mathbf{S}$  and  $\mathbf{T}$  are vectors of length NS1, NS1, NS2, NS2 and NS3, respectively, which contain the unknown amplitudes of the virtual sources of the MFS. Each entry of  $\mathbf{A}$ ,  $\mathbf{x}$  and  $\mathbf{B}$  corresponds, itself, to a submatrix containing the effects of each set of virtual sources on each boundary. The matrices  $\mathbf{G}$  and  $\mathbf{H}$  can be written as:

$$\mathbf{G}_{\Gamma_i,j,\Omega_l} = \begin{bmatrix} G^{3D}(\bar{\mathbf{x}}_{1,\Gamma_i}, \mathbf{x}_{j,1}, k_l) & \cdots \\ \vdots & \\ G^{3D}(\bar{\mathbf{x}}_{NSi,\Gamma_i}, \mathbf{x}_{j,1}, k_l) & \cdots \\ \cdots & G^{3D}(\bar{\mathbf{x}}_{1,\Gamma_i}, \mathbf{x}_{j,NSj}, k_l) \\ \vdots & \\ \cdots & G^{3D}(\bar{\mathbf{x}}_{NSi,\Gamma_i}, \mathbf{x}_{j,NSj}, k_l) \end{bmatrix} \quad (13)$$

$$\mathbf{H}_{\Gamma_i,j,\Omega_l} = \begin{bmatrix} H^{3D}(\bar{\mathbf{x}}_{1,\Gamma_i}, \mathbf{x}_{j,1}, k_l, \bar{\mathbf{n}}_{1,\Gamma_i}) & \cdots \\ \vdots & \\ H^{3D}(\bar{\mathbf{x}}_{NSi,\Gamma_i}, \mathbf{x}_{j,1}, k_l, \bar{\mathbf{n}}_{NSi,\Gamma_i}) & \cdots \\ \cdots & H^{3D}(\bar{\mathbf{x}}_{1,\Gamma_i}, \mathbf{x}_{j,NSj}, k_l, \bar{\mathbf{n}}_{1,\Gamma_i}) \\ \vdots & \\ \cdots & H^{3D}(\bar{\mathbf{x}}_{NSi,\Gamma_i}, \mathbf{x}_{j,NSj}, k_l, \bar{\mathbf{n}}_{NSi,\Gamma_i}) \end{bmatrix} \quad (14)$$

where  $\bar{\mathbf{x}}_{n,\Gamma_i}$  represents the collocation point  $n$  over boundary  $\Gamma_i$ ,  $\mathbf{x}_{j,n}$  is the virtual source  $n$  associated with  $j^{th}$  set of virtual sources,  $NSi$  is the number of collocation points over boundary  $\Gamma_i$ ,  $k_l$  is the wavenumber in domain  $\Omega_l$ , and  $\bar{\mathbf{n}}_{m,\Gamma_i}$  is the normal to boundary  $\Gamma_j$  at the  $m^{th}$  collocation point. Finally, the independent term  $\mathbf{B}$  contains the effects of a possible real acoustic source at each of the collocation points. Further details will be given in the next subsection.

After solving the equation system, the

475 pressure at any point of the host water domain can be determined making use of Equation (4).

One should note that this formulation can be greatly simplified if only some 480 of the features of the fish are to be considered. In those cases, a careful selection of the correct subsets of virtual sources can lead to a significant reduction of the size of the equation 485 system. The cases of interest for this paper are:

- Considering just the spine and swimbladder: for this case, only the interfaces  $\Gamma_2$  and  $\Gamma_3$  are 490 needed, as well as the third, fourth and fifth virtual source sets, leading to a system with  $2 \times NS_2 + NS_3$  equations and unknowns; the required 495 boundary and interface conditions are given by equations (9), (10) and (11);
- Only considering the swimbladder: in this case, only 500 the boundary  $\Gamma_3$  is required, and the fifth virtual source set is sufficient to simulate the sound field in the host medium, leading to a system with  $NS_3$

505 equations and unknowns; the required boundary conditions are given by equation (11).

### 2.1.3. Simulation of the acoustical transducer and beam in the far 510 field.

As mentioned above, the independent term in Equation (12) contains the effect of the real source, illuminating the scatterers. This source can be of any 515 type, such as a simple point load, or can be a more complex and realistic radiating object. For the purpose of the present paper, the specific case of the far field of a circular piston, as an 520 idealisation of a scientific echosounder transducer, is of particular interest, since this is the usual tool used in practice to create the incident acoustic signal in field measurements.

525 To simulate this type of source, its surface is first discretized in small triangles, as illustrated in Figure 2, and the necessary boundary conditions are prescribed at each of these triangles 530 (usually a given particle velocity at the emitting surface, and null velocity at the remaining surfaces). Assuming that the source is sufficiently far from the scatterer and considering that high

535 frequencies are excited, a high-frequency approximation of the sound field at the required field points can then be obtained using the Rayleigh integral in the form

$$540 \quad p(\mathbf{x}, k_1)_{\Omega_1} = 2i\omega\rho \times \int_{\Gamma_{source}} G^{3D}(\mathbf{x}_{\Gamma_{source}}, \mathbf{x}, k_1) v(\mathbf{x}_{\Gamma_{source}}, k_1, \vec{n}) \quad (15)$$

This simple approach can be computationally very effective, since it does not require the solution of any equation system. However, one should 545 note that this can only be considered for high frequencies and for small sources, where the interaction between the source and the scatterers can be neglected.

## 550 2.2 Verification of the MFS for a fluid-filled sphere.

To first verify the proposed MFS formulation, the benchmark case of a fluid-filled sphere subject to the 555 incidence of a plane wave is considered.

For that purpose, a sphere with radius 0.01 m is defined, immersed in water with  $c=1479.6$  m/s and  $\rho=1027$  kg/m<sup>3</sup>., and three different sets of properties are 560 considered for the fluid filling the sphere:

-  $c = 343$  m/s and  $\rho = 1.2$  kg/m<sup>3</sup> , simulating air;

-  $c = 1520$  m/s and  $\rho = 1043$  kg/m<sup>3</sup> , 565 simulating the properties of fish flesh;

-  $c = 5000$  m/s and  $\rho = 7000$  kg/m<sup>3</sup> , simulating a quasi-rigid sphere.

All three cases are analysed for incident 570 plane waves with frequencies of 38 kHz or 120 kHz, and for increasing numbers of uniformly distributed collocation points defining the sphere, ranging from 100 to 1500. For each number of 575 collocation points, a relative error is computed with respect to the classical benchmark analytical solution given by Andersen [45], taking into account the response at a receiver located 0.02m 580 from the centre of the sphere.

Figure 3 presents the relative error at the receiver for the three configurations described before. It can be observed that fast convergence is registered for all the 585 properties of the inner fluid, with very low errors being computed for as little as 300 collocation points, even at the higher excitation frequency. To have a better insight of the meaning of these 590 results, in the same figures,

convergence curves computed for a conventional BEM implementation were also included. Clearly, comparing both methods, the MFS provides a much faster convergence to the solution, allowing an effective reduction of the number of collocation points to provide the same error level as the BEM.

### 2.3 Application of MFS to calculate the TS of a gas-filled prolate spheroid.

A comparison of well-established numerical models for TS estimation of swimbladdered fish was given in [20]. In the cited work it was considered the acoustic reflection from pressure release prolate spheroids, which approximate a fish swimbladder [6,46]; results obtained from the analytically exact prolate-spheroid-modal-series model (PSMS) were compared with the computed results from KA, KRM and FEM. We have applied the MFS formulation introduced in the previous subsection to the same cases of gas-filled prolate [20] with semi-major axis  $a$  [m] and semi-minor axis  $b$  [m]. To compare with [20] we have calculated length-normalized TS as  $nTS =$

$10 \log_{10} \left( \frac{R^2 I_{bs}}{a^2 I_{inc}} \right)$  [dB], where  $I_{bs}$  [ $\text{W m}^{-2}$ ] corresponds to the backscattering from the target calculated on the ultrasonic source;  $R$  [m] is the distance between the target and the source and  $I_{inc}$  [ $\text{W m}^{-2}$ ] is the incident intensity on the target. Following [20] we have chosen two prolate spheroids with  $ka = 12$  and  $kb = 1$  or  $kb = 5$ , where  $k$  is the acoustic wavenumber, given by  $2\pi f/c$ . For each prolate spheroid, the length-normalized TS have been calculated at incident angles from 0 to 50, in 2 degree steps. Sound velocity  $c$  in water surrounding the prolate spheroid is 1479.6 m/s and density  $\rho=1027 \text{ kg/m}^3$ . Since the gas filling the swimbladder ( $c=343 \text{ m/s}$  and  $\rho=1.2 \text{ kg/m}^3$ ) exhibits a very large contrast with the water, null pressure conditions are ascribed to the boundary of the prolate spheroid. The working acoustic frequency was set to 38 kHz and the prolate spheroid dimensions were chosen to obtain the required  $ka$  and  $kb$  values.

### 2.4. Relative contributions of fish elements.

As it was stated previously in the paper, the usual properties that can be

650 considered for the fish flesh are closer to those of the host fluid medium (water) than other fish structures, and so the perturbation in the response originated by the contrast of properties between water and flesh should be a minor contribution in comparison with the swimbladder or the spine. However, confirmation of this hypothesis is necessary, and so, to assess the influence of considering different levels of detail of the fish model in the calculation of the TS, simulations were performed using the proposed MFS model. In these simulations, the flesh is assumed to have  $c = 1520$  m/s and  $\rho = 1043$  kg/m<sup>3</sup>, and the spine is assumed to have  $c_{bone} = 2270$  m/s,  $\rho_{bone} = 1100$  kg/m<sup>3</sup>. A small fish of length 0.18 m is considered, with a spine length of 0.15 m.

Using the described problem configuration, simulations were performed using the 3D MFS model and considering three distinct situations: the complete fish with the fish flesh, the fish represented by its spine and swim bladder, or just including the swim bladder. Two different frequencies were analysed, 70 kHz and 120 kHz, and the

680 TS was computed for ventral and dorsal insonification considering distances ranging from 1.0 m to 10.0 m.

### 2.5. Application of the MFS to calculate the compared gains of the TS from a swimbladder fish (Atlantic salmon) depending on aspect.

Once the MFS has been applied to the calculation of the TS of an idealised fish, we wanted to improve the understanding of TS measurements of big- and medium-sized fish at short distances when the far field condition for the emitted acoustic beam is assured. In particular we focused on the TS results obtained in [13] for the ventral and dorsal aspects of Atlantic salmon introduced above.

Teleost fish, such as salmon, normally have a swimbladder. This organ, located below the fish bone, is responsible for most of the energy reflected by the fish [43]. Therefore, in principle, ventral and dorsal TS measurements would only differ in the influence of shapes and orientation of swimbladder boundaries and minor backscattering, diffraction and shadowing effects of the fish bony structures (spine) [26,47]. We have

710 considered a simplified scheme of Atlantic salmon, shown in Figure 1.a), to evaluate the differences when measuring dorsally or ventrally and their influence in the near field distance 715 of the scattered field from the fish. Since the flesh and the skull would contribute in a similar way to the total TS from both insonification perspectives, their contributions were 720 not taken into account to simplify the calculations.

The emitting transducer was modelled as a flat piston as explained above and we calculated the evolution of the 725 measured TS with distance and with relative orientation between the transducer axis and fish for the case of 120 kHz. For the sake of comparison, we calculated as well for a lower 730 frequency, 70 kHz, since the required computational memory exceeded our hardware limits at 200 kHz (64 GB). The transducer size was chosen to produce a half-beam angle at -3dB of 735  $3.5^\circ$  following the transducers' specifications of Simrad EK60 scientific echosounders at the working frequencies. We considered ventral and dorsal insonifications of fish in order to 740 analyse the effect of the spine in the

near-to-far field evolution of the backscattered field in each configuration. We considered ventral and dorsal insonifications of fish in 745 order to analyse the effect of the spine in the near-to-far field evolution of the backscattered field in each configuration. The simulated TS derives from the value of the 750 backscattered field at the position of the transducer working as a receiver, like in real measurements. Since the TS is calculated as the logarithmic expression of the ratio between the backscattered 755 intensity at 1 m of the scatterer and the incident intensity on it, we must compensate the transmission loss from this distance to the transducer, considering absorption and the 760 geometrical decay. As it is done by the software implemented in scientific echosounders, the scatterer is considered in the far field as a point source with a geometrical decay of 20 765  $\log R$ . If this fish far-field condition is achieved, the resulting TS will not vary with fish distance. Therefore in the near field of fish the measurements (and our simulations) will exhibit TS variations, 770 whilst the far field condition can be assumed when the TS reaches a certain



stationary value. In these calculations we have assumed the following properties for the materials:  $c_{bone} = 2270$  775 m/s,  $\rho_{bone} = 1100 \text{ kg/m}^3$ ,  $c_{water} = 1479.6$  m/s and  $\rho_{water} = 1027 \text{ kg/m}^3$  [48,49]; since the fishbone is modelled as a fluid-like structure, only longitudinal wave propagation across the fishbone 780 has been considered.

The relation between spine and swimbladder dimensions, as well as the relative tilting angle, for a fish of total length  $L$  ( in cm), has been chosen to 785 approximate the internal structure of Atlantic salmon [29,50,51].

To compare with the experimental results in [13] we performed the calculations for fish lengths,  $L$ , from 24 790 up to 72 cm, corresponding to spine lengths from 20 to 60 cm. We have simulated measuring distances from transducer to fish from 6 to 100 meters, and the distance range from 6 to 18 795 meters is separately analysed in 1 m steps to compare with [13]. To take into account fish behaviour when diving and surfacing, TS directivity has been calculated at each measuring distance 800 for a fish rotation from -90 to 90 degrees, considering angular intervals

of 1 degree, for both 70 and 120 kHz.

### 3. Results

#### 805 3.1. Fluid-like sphere

The case of the fluid-filled sphere illuminated by a plane wave, for which analytical solution is known, can be quite useful to assess capacity of the 810 MFS model to reproduce the acoustic pressure field at different distances from the scatterer.

To have an adequate insight on the behaviour of the method, results 815 presented in Figure 4 illustrate, for the three scenarios identified in section 2.2, a comparison between the analytically and numerically computed sound pressures over a line of receivers 820 crossing the sphere, and positioned between  $x = -0.3\text{m}$  and  $0.3\text{m}$ . The system is illuminated by a plane wave propagating parallel to the  $y$ - $z$  plane, in the negative direction of the  $x$  axis, and 825 frequencies of 38kHz and 120kHz are considered.

The comparison between the MFS and the analytical solution reveals an excellent agreement between both

830 results, for all computed distances. The analysis of these results indicates that the MFS can reproduce both the near field and the far field of the scatterer with excellent accuracy, and ensures 835 that the method can be used for the analysis of more complex cases, both in what concerns the near field and the far field of scatterers.

### 3.2. TS of a gas-filled prolate 840 spheroid with MFS.

Figure 5 compares the result from MFS with the exact analytical solutions from PSMS; and with the numerical solutions of KA, KRM and FEM. Figure 5 845 reproduces *Figure 4* in [31], modified to include our results from MFS calculations.

To analyse the computational performance of the MFS in this type of 850 problem, in comparison with BEM, the two extreme geometries of prolate spheroids of [20] were considered; with lengths of 14.74 cm and 14.84 cm, and transverse diameter of 1.24 cm and 6.18 855 cm, as depicted in Figure 6. For both configurations, the spheroid is illuminated by a circular piston of radius 3.1 cm, located 10 m away from the scatterer, working at a frequency of

860 38 kHz. Figure 7 depicts polar plots comparing the MFS and the BEM TS directivity results for these configurations.

### 3.3. Influence of the different 865 structures of fish in the computed TS.

The calculated TS for ventral insonification of a small fish, of length equal to 0.18 m (spine length of 0.15m), 870 is represented in Figures 8a and 9a, as a function of the distance between the transducer and the fish, while dorsal insonification results are presented in Figures 8b and 9b. Transducers with 875 two different frequencies are considered, with the TS for a 70 kHz transducer being represented in Figure 8, and the TS for a 120 kHz transducer being depicted in Figure 9. In each figure, 880 three curves are represented, corresponding to the calculation considering the complete fish model including the flesh (dashed line with circle marks), just considering the spine 885 and swim bladder (dashed line with star marks), and only accounting for the swim bladder (dotted line with square marks).

### 3.4. Case study with MFS: TS of Atlantic salmon in floating cages.

#### 3.4.1. TS directivity.

The  $TS(\theta)$  directivities, being  $\theta$  the observation angle, at 70 and 120 kHz are given in Figure 10 for  $L=24$  cm and  $L=72$  cm fish size at 6 m and 18 m from the transducer, corresponding to the limits of the selected distance range in [13].

The calculations compare the results from ventral and dorsal fish aspect, varying the observation angle  $\pm 90^\circ$ , from the normal incidence, the positive x-axis has been taken to be  $\theta=0$ .

The directivity of the fish,  $TS(\theta)$ , was calculated at different target-to-transducer distances and the maximum value of  $TS(\theta)$ , defined as  $TS_{max}(d)$ , for each fish-to-transducer distance,  $d$ , was obtained for further analysis.

#### 3.4.2. $TS_{max}$ versus fish-to-transducer distance.

The variation of the maximum value of TS,  $TS_{max}$ , with the target-to-transducer distance is shown in Figure 12. It should be noted that only distances in the far-field regime of the transducers are considered. Fig. 11

shows that the value of  $TS_{max}$  reaches a constant value, defined as  $TS_{FF}$ , only from a far enough distance. For larger fish the constant  $TS_{max}$  value is reached further than for smaller ones. Dorsal aspect calculations resulted in minor  $TS_{max}$  values and further distances to get  $TS_{FF}$  than ventrally. Distance to reach  $TS_{FF}$  also increased with frequency.

#### 3.4.3. $TS_{max}$ and fish length

Figure 12 provides the regression curves showing the  $TS_{max}$  value dependence on the fish length when ventral fish aspect is considered. The fish-to-transducer distance has been fixed to  $d=18$ m, corresponding to Eq. (13) for 70 kHz and Eq. (14) for 120 kHz. In order to compare with experimental results, the mean TS versus logarithm of length relationship from the regression linear fit given in [13] has been included. Good correlations were obtained ventrally both at 70 kHz and 120 kHz:

$f = 70$  kHz; ventral fish aspect:

$$TS_{max} = 19.1 \log_{10}(L) - 58.82, \quad (13)$$

$f = 120$  kHz; ventral fish aspect:

$$TS_{max} = 18.18 \log_{10}(L) - 57, \quad (14)$$

where  $TS_{max}$  is measured in dB and  $L$  in cm, with correlation coefficients  $R^2 = 0.98$  in both cases. Ventrally, from 6 to 18 meters, as considered in 950 [13], the relationship between  $TS_{max}$  and fish length exhibited very good correlation, with  $R^2 \geq 0.97$ .

However, dorsal aspect simulations provided poorer  $TS_{max}$ -to-logarithm-955 of-fish-length correlations along the distance range of measurements in [13], mainly for the higher frequency. At  $d = 18$  m the dorsal TS vs. L relationship was given by

960  $f = 70$  kHz; dorsal fish aspect:

$$TS_{max} = 12.88 \log_{10}(L) - 50.24, \quad (15)$$

$f = 120$  kHz; dorsal fish aspect:

$$TS_{max} = 7.4 \log_{10}(L) - 44.01, \quad (16)$$

with correlation coefficients  $R^2 = 0.94$ 965 and  $R^2 = 0.7$  respectively. From 6 to 18 m, the relationship between  $TS_{max}$  and fish length exhibited good correlation and expected values only for the lower frequency, with  $0.9 \geq R^2 \geq$ 970  $0.94$  at 70 kHz and  $0.47 \geq R^2 \geq 0.7$  at 120 kHz. Nevertheless, when the calculations were performed to distances where the far field is supposed to be achieved (arbitrarily 100 m), the

975 results show good correlations both for ventral and dorsal aspects of fish. The dependence of  $TS_{max}$  with fish length for 120 kHz at 100 m of the transducer were given by:

$f = 120$  kHz; (ventral fish aspect):

$$980 TS_{max} = 18.29 \log_{10}(L) - 56.9, \quad (17)$$

$f = 120$  kHz; (dorsal fish aspect):

$$TS_{max} = 13.96 \log_{10}(L) - 53.34, \quad (18)$$

with correlation coefficients  $R^2 = 0.99$  and  $R^2 = 0.98$  respectively. Similar 985 results could be found at 70 kHz.

## 4. Discussion

### 4.1. Verification of the proposed MFS model for numerical calculation

990 of TS.

There was a good agreement between the MFS results and the analytical solutions of all fluid-like spheres and the PSMS method in all prolate 995 spheroid sizes and inclinations considered, similar or even better to the results obtained with FEM (Figure 5). The most important disadvantage of FEM model is the large computational requirements for three-dimensional 1000 problems and long propagation

distances, even more if we consider the higher frequencies which increase the needed mesh density. Nevertheless, MFS is a meshless method, which means that we can avoid some limitations found with a FEM model due to fine mesh requirements. If we compared the results for backscattering acoustic field from a prolate spheroid calculated with FEM and MFS models, we could conclude that using MFS model we kept good agreement with PSMS model, but the computational effort was reduced, even more when higher frequencies were considered. A similar argument supports the use of BEM for such calculations. However, if we take into account the results shown in Figure 3 for fluid-filled spheres, it was clear that the accuracy of the MFS can be better than that of the BEM, allowing reduction in the number of points to reach the same accuracy level. Considering the polar plots from Figure 7 (calculated for the prolate spheroids in Figure 6), they also indicated an excellent agreement between MFS and BEM results for non-spherical geometries. The BEM is well-known for its high accuracy and reliability, and so this was a quite important finding

that allows us to state that the MFS was also able to provide accurate results for this type of regular geometry. Since both BEM and MFS use equal number of elements (BEM) and collocation points (MFS) in the presented example, and thus led to similar RAM memory requirements, it is interesting to compare their computational performance. When calculated in a PC equipped with an Intel i7-4790 @3.6GHz, calculation times of 3.4s and 1.6s were obtained for the MFS, and of 5.9s and 2.8s for the BEM. Thus, for the two studied cases, the MFS consistently allowed a reduction in the calculation time, which was around 55%-60% of that obtained using the BEM.

The result in Figure 5 verified that MFS was a valid method for estimating the TS of swimbladdered fish. In addition, results shown in Figure 4, also clarified that the method was capable of simulating the pressure field both near and far from the scattering fish with accuracy. It is clear that MFS model also has limitations to be used for TS calculations. The number of nodes on the target surface as well as the number of virtual sources determines the dimension of the matrix. The dimension

of the matrix constrains the application  
 1065 of the model. Matrix dimension  
 increases with the target size, the  
 frequency and the number of domains  
 (interfaces with different materials)  
 composing the target, and it is  
 1070 dependent on shape of the domains. As  
 explained in the introduction, MFS is  
 more adequate for soft-rounded shapes,  
 since sharp edges can affect its accuracy.  
 These factors could restrict the  
 1075 application of MFS to TS simulations,  
 in close competition with BEM. BEM is  
 in principle useful for arbitrary shapes,  
 even those with sharp edges; this also  
 implies to define the shape boundaries  
 1080 with a higher number of elements, and  
 the consequent increase of  
 computational memory needs. Globally,  
 the MFS is a good candidate to estimate  
 TS of simplified smooth structures form  
 1085 near to far field, even for higher  
 frequencies, with a lower computational  
 effort than the BEM for the same  
 geometries.

One relevant aspect that is worth  
 1090 discussing is related to the importance  
 of incorporating or not the fish flesh in  
 the conceptual fish model. The results  
 depicted in Figures 8 and 9, calculated  
 using 3D MFS models considering the

1095 complete fish (including the flesh), the  
 spine and the swimbladder, and only the  
 swimbladder, clearly shown that  
 considering the spine in the numerical  
 model introduces some important  
 1100 changes for both frequencies, while the  
 effect of the flesh, for the tested cases,  
 particularly with ventral insonification,  
 was less significant; from the presented  
 plots, maximum deviations of around  
 1105 0.2 dB were registered for the lower  
 frequency, and even lower deviations  
 were seen for 120 kHz, with the  
 introduction of the fish flesh in the  
 model. However, the computational  
 1110 effort required to consider the presence  
 of the fish flesh was considerably  
 higher: for example, in the model used  
 for 120 kHz insonification, an equation  
 system with 44528 equations and 44528  
 1115 unknowns needed to be assembled in  
 order to consider the fish flesh; if just  
 the swim bladder and the spine were  
 modelled, the dimension of this system  
 was drastically reduced to 5704  
 1120 equations and 5704 unknowns. Given  
 the very small differences of TS  
 introduced by the flesh, and also the  
 fact that no qualitative changes are  
 observed in the plots between the two  
 1125 situations, we believe that the

simplification of the model to just consider the spine and the swimbladder provided physically meaningful results, and it was adequate for the analysis of 1130 TS by swimbladdered fishes for the analysed frequencies. A similar consideration should be done about considering the skull in the fish model: The obtained results are representative 1135 of the simplified model and incorporating the skull may modify the absolute TS response, but in a similar way for dorsal and ventral insonifications.

#### 1140 4.2. Case study: Atlantic salmon in floating cages.

##### 4.2.1. TS directivity

Because of the tilted swimbladder, the backscattering direction is not 1145 necessarily the direction corresponding to the maximum value of TS, even when fish swim horizontally. The calculations show qualitatively different directivity results for dorsal and ventral 1150 aspects, exhibiting more complex structure in the dorsal configuration. For a fish of 24 cm, the directivity was mostly the same both at 6 and 18 m. Then it can be considered that 1155 measurements in [13] were performed

far enough to be in the far-field region of the target for such fish size. Nevertheless, in the case of a bigger fish ( $L=72$  cm), the directivity changed 1160 along the distance range considered in [14], for the case of dorsal configuration at 120 kHz (Figure 10). As it was expected, directivity increased with frequency [27], which was clearly 1165 shown comparing the results at 70 and 120 kHz for dorsal calculation: the presence of lobes could be observed, being narrower for the larger target. For the smaller target the existence of lobes 1170 could contribute to the appearance of bi- or tri-modal TS distributions in measurements. However, it was possibly not enough to explain them completely, and the specific shape of 1175 the swimbladder and/or the fish bone should be considered to describe them properly, as has been suggested by [13]. By instance, the modulation of the spine shape should introduce variability and a 1180 softening effect in the coherent modulation of directivities noticeable in Figure 10.

##### 4.2.2. $TS_{max}$ and fish-to-transducer distance

1185

Our calculations showed that the fish-to-transducer distance to get the far-field region depends not only on the fish size, but also on the fish aspect considered. The dependence on the fish aspect is more evident in the case of large fish (see Figure 11). We focus now in our results at 120 kHz, to compare with experimental measurements of [13]: for ventral calculations,  $TS_{max}$  variations with measuring distance are less than 1% in the measuring interval –from 6 to 18 meters- and less than 5% when the  $TS_{max}$  value at 6 meters is compared with the  $TS_{max}$  value at 100 m, where the far field condition should have been reached. Nevertheless, for dorsal aspect calculations, those variations are as large as the 8% along the measuring interval and reaching variations of 16% between the value at 6 and 100 meters. From Figure 11, it is evident that the far-field distance also moves further for dorsal than for ventral aspect simulations.

It should be remarked that the different behaviour between dorsal and ventral simulations comes exclusively from the presence of the bone, and not from the particular morphometry of the

swimbladder, what was proposed to be the main cause of the divergence between ventral and dorsal measurements [13]. Ventrally, the acoustic wave impinges almost directly on the swimbladder – with a minor effect of the fish flesh. Dorsally, however, the ultrasonic field impinges first on the fish spine, which shadows the swimbladder and diffracts the field. Ventrally, and perhaps laterally, the Fraunhofer distance is governed by the swimbladder dimension [6, 16]. On the contrary, the total length of the fish spine should be considered for dorsal configurations. This could also explain why ventral  $TS_{max}$  exhibits higher values than dorsal  $TS_{max}$  [13, 52, 53]: the secondary scattering by the swimbladder has been shadowed because of the presence of the spine. Higher  $TS$  values in ventral measurements than in dorsal have been also reported in measurements on other species with swimbladder: bluefin tuna *Thunnus thynnus* [14] and gilt-head sea bream *Sparus aurata* [54]. Both the divergence in far-field distance between dorsal and ventral configurations and the higher  $TS$  values for ventral rather than for dorsal fish aspect would be



revealed as a universal feature for fish species possessing swimbladder.

1250

#### 4.2.3. *TS*max and fish length

The good correlation obtained between ventral calculations and measurements at short distances, rather than dorsally, could be also interpreted as a consequence of the diffraction effects of fishbone. The presence of the spine distorts the acoustic field, as can be observed comparing dorsal and ventral directivity diagrams in Figure 10. The coherent effects of the superposition of the contributions of bladder and spine were revealed in those plots. A more realistic description of the spine geometry should produce a smoothing of the smaller scales in the directivity patterns.

The far field region was further away in the dorsal measurements case and the relationship between *TS* and fish length showed, indeed, poorer correlation coefficients at short distances. Nevertheless, for large enough distances the good correlation of *TS* versus fish length was recovered and then we could assume that the far field condition has been achieved. The relationship

between ventral *TS*max and fish size with a good correlation coefficient was achieved closer to the target than for the dorsal case.

1280

This was apparently contradictory with the results of *TS* variation with distance reported in [13]. But it should be remarked that, for each fish length, the variations of simulated *TS*max with distance between 6 and 18 meters are in the variation range of the measured mean *TS* reported by [13],

$$1290 TS_{max}(d) = (0 \pm 0.2)(d - 6) +$$

$TS_{max_6}$ , where  $TS_{max_6}$  is the *TS*max value calculated at 6 meters from the fish.

## 1295 5. Conclusions

The MFS can be a very useful tool for estimating the measurable *TS* of fish at arbitrary close distances, taking into account the effect of the near field of fish and the contribution to *TS* of fish main structures. The application of MFS has been verified against the most recognized numerical methods showing a better performance in computational terms than BEM for idealised smooth geometries.

The coherent contribution of the different inner structures of fish can be considered using MFS, and for the case of swimbladdered fish, the main features of the evolution with distance of the backscattered field are described considering a simplified fish model that takes into account only the bladder and the spine.

The presented numerical results would suggest that ventral measurements are able to give more reliable and higher TS values at short distances than dorsal measurements; a common experimental condition in aquaculture cages. The effect of fish bone is relevant when dorsal fish aspect is considered: it influences on the far-field distance, leads to lower TS value and poorer correlation of TS versus fish size at short distances. The present numerical simulation could aid in interpreting the divergences between ventral and dorsal measurements reported in [13, 14, 52-54]. To reproduce quantitatively the experimental results of [13] a synthetic reproduction of TS distributions should be obtained, considering appropriate fish distance and tilt distributions. Also, the effect of a more detailed description of swimbladder and fishbone geometry

should be considered.

## Acknowledgements

I. Pérez-Arjona and V. Espinosa acknowledge funding of ACUSTUNA project ref. CTM2015-70446-R (MINECO/ FEDER, UE), and UPV grants of PAID-00-15 and GVA BEST/2015/270. L. Godinho acknowledges the funding by FEDER funds through the Competitvity Factors Operational Programme - COMPETE and by national funds through FCT – Foundation for Science and Technology within the scope of the project POCI-01-0145-FEDER-007633. The authors would like to thank Dr. Manuel Bou and Carlos Albino for the technical assistance with workstation procedures.

## References

- 1 D.N. MacLennan, E. J. Simmonds: Fisheries acoustics: theory and practice. Blackwell Science, 2005.
- 2 K.G. Foote: Summary of methods for determining fish target strength at ultrasonic frequencies. ICES

- Journal of Marine Science: 211-217.
- Journal du Conseil 48.2 (1991): 211-217.
- 3 D.N. MacLennan: Time varied gain 1400  
1370 functions for pulsed sonars. Journal of Sound and Vibration 110.3 (1986): 511-522.
- 4 K. Foote, H. Knudsen, G. Vestnes, D. MacLennan, E. Simmonds: 1405 9  
1375 Calibration of acoustic instruments for fish density estimation: a practical guide No. 144. International Council for the Exploration of the Sea, 1987. 1410
- 1380 5 E. Ona, K.G. Foote, X. Zhao, I. Svellingen: Some Pitfalls of Short-Range Standard-Target Calibration. ICES 1996. 1410
- 6 M. Furusawa: Prolate spheroidal 1415 11  
1385 models for predicting general trends of fish target strength. Journal of the Acoustical Society of Japan (E) 9.1 (1988): 13-24.
- 7 M. Moszyński, A. Stepnowski: 1420  
1390 Increasing the accuracy of time-varied-gain in digital echosounders. Acta Acustica united with Acustica 88.5 (2002): 814-817. 1425
- 1395 8 A. Bertrand, E. Josse, and J. Massé: In situ acoustic target-strength measurement of bigeye (Thunnus obesus) and yellowfin tuna (Thunnus albacares) by coupling split-beam echosounder observations and sonic tracking. ICES Journal of Marine Science: Journal du Conseil 56.1 (1999): 51-60.
- 9 J. Dawson, D. Wiggins, D. Degan, H. Geiger, D. Hart, B. Adams: Point-source violations: split-beam tracking of fish at close range. Aquatic Living Resources 13.5 (2000): 291-295
- 10 T.J. Mulligan: Shallow water fisheries sonar: a personal view. Aquatic Living Resources 13.5 (2000): 269-273.
- 11 R. Kieser, T. Mulligan, J. Ehrenberg: Observation and explanation of systematic split-beam angle measurement errors. Aquatic Living Resources 13.5 (2000): 275-281.
- 12 S.J. Fleischman, D.L. Burwen: Correcting for position-related bias in estimates of the acoustic backscattering cross-section. Aquatic Living Resources 13.5 (2000): 283-290.
- 13 F.R. Knudsen, J. Fosseidengen, F.

- Oppedal, Ø. Karlsen, E. Ona: Hydroacoustic monitoring of fish in sea cages: target strength (TS) measurements on Atlantic salmon (*Salmo salar*). Fisheries research 69.2 (2004): 205-209.
- 14 V. Puig, V. Espinosa, E. Soliveres, A. Ortega, A. Belmonte, F. de la Gándara: Biomass estimation of bluefin tuna in sea cages by the combined use of acoustic and optical techniques collect. Collect. Vol. Sci. Pap. ICCAT 68 (2012)..
- 15 H.J. Lu, M. Kang, H.H. Huang, Ch.Ch. Lai, Ch.Ch. Wu: Ex situ and in situ measurements of juvenile yellowfin tuna *Thunnus albacares* target strength. Fisheries science 77.6 (2011): 903-913.
- 16 V. Rodríguez-Sánchez, L. Encina-Encina, L. Rodríguez-Ruiz, R. Sánchez-Carmona: Fisheries Research 173 (2016): 4-10.
- 17 G.D. Melvin: Observations of in situ Atlantic bluefin tuna (*Thunnus thynnus*) with 500-kHz multibeam sonar. ICES Journal of Marine Science: Journal du Conseil (2016): fsw077.
- 18 G. Moreno, G. Boyra, I. Rico, I. Sancristobal, J.D. Filmater, F. Forget, J. Murua, N. Goñi, H. Murua, J. Ruiz, J. Santiago, V. Restrepo: Towards acoustic discrimination of tuna species at FADs. Collect. Vol. Sci. Pap. ICCAT 72 (2016): 697-704.
- 19 R.W.G:Haslett: Acoustic backscattering cross sections of fish at three frequencies and their representation on a universal graph, British journal of applied physics 16.8 (1965): 1143.
- 20 G.J. Macaulay, H. Peña, S.M. Fässler, G. Pedersen, E. Ona: Accuracy of the kirchhoff-approximation and kirchhoff-ray-mode fish swimbladder acoustic scattering models. PloS one 8.5 (2013): e64055.
- 21 J.M. Jech, J.K. Horne, D. Chu, D.A. Demer, D.T.I. Francis, N. Gorska, B. Jones, A.C. Lavery, T.K. Stanton, G.J. Macaulay, D.B. Reeder, K. Sawada: Comparisons among ten models of acoustic backscattering used in aquatic ecosystem research. The Journal of the Acoustical Society of America 138.6 (2015): 3742-3764.
- 22 P.C. Waterman: The Journal of the

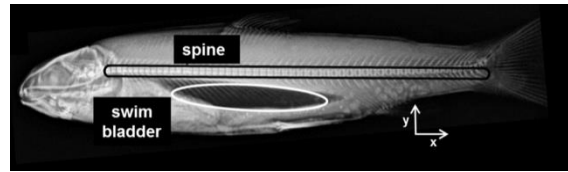
- 1490 Acoustical Society of America  
45.6 (1969): 1417-1429.
- 23 T.K. Stanton: Sound scattering by  
cylinders of finite length. III.  
Deformed cylinders. The Journal 1525  
of the Acoustical Society of  
America 86.2 (1989): 691-705.
- 1495 24 M.A. Do, A.M. Surti: Estimation of  
dorsal aspect target strength of  
deep-water fish using a simple 1530  
model of swimbladder  
backscattering. The Journal of the  
Acoustical Society of America  
87.4 (1990): 1588-1596.
- 1500 25 Z. Ye: A novel approach to sound 1535  
scattering by cylinders of finite  
length. The Journal of the  
Acoustical Society of America  
102.2 (1997): 877-884.
- 1510 26 K.G.Foote: Rather-high-frequency 1540  
sound scattering by  
swimbladdered fish. Journal of  
the Acoustical Society of America  
78 (1985): 688–700.
- 1515 27 C.S. Clay, J.K. Horne: Acoustic 1545  
models of fish: The Atlantic cod  
(*Gadus morhua*). The Journal of  
the Acoustical Society of America  
96.3 (1994): 1661-1668.
- 1520 28 D.B. Reeder, T.K. Stanton: Acoustic 1550  
scattering by axisymmetric finite-  
length bodies: An extension of a  
two-dimensional conformal  
mapping method. The Journal of  
the Acoustical Society of America  
116.2 (2004): 729-746.
- 29 J. Lilja, T. Marjomäki: Jurvelius J,  
Rossi T, Heikkola E. Simulation  
and experimental measurement of  
side-aspect target strength of  
Atlantic salmon (*Salmo salar*) at  
high frequency. Canadian Journal  
of Fisheries and Aquatic Sciences  
61.11 (2004): 2227-2236.
- 30 K.G. Foote, D.T.I. Francis:  
Comparing Kirchhoff-  
approximation and boundary-  
element models for computing  
gadoid target strengths. The  
Journal of the Acoustical Society  
of America 111.4 (2002): 1644-  
1654.
- 31 K.G. Foote KG, J.J Traynor:  
Comparison of walleye pollock  
target strength estimates  
determined from *in situ*  
measurements and calculations  
based on swimbladder form The  
Journal of the Acoustical Society  
of America 83.1 (1988): 9-17.
- 32 E.L. Hazen, J.K. Horne: Comparing  
the modelled and measured target-

- strength variability of walleye pollock, *Theragra chalcogramma*. ICES Journal of Marine Science: 1585
- 1555 Journal du Conseil 61.3 (2004): 363-377.
- 33 D.B. Reeder, J.M. Jech, T.K. Stanton: Broadband acoustic backscatter and high-resolution morphology of fish: Measurement and modeling. The Journal of the Acoustical Society of America 116.2 (2004): 747-761.
- 1560
- 34 M.J. Henderson, J.K. Horne: Comparison of in situ, ex situ, and backscatter model estimates of Pacific hake (*Merluccius productus*) target strength. Canadian Journal of Fisheries and Aquatic Sciences 64.12 (2007): 1781-1794.
- 1570
- 35 J.M. Jech, D.M. Schael, C.S. Clay: Application of three sound scattering models to threadfin shad (*Dorosoma petenense*). The Journal of the Acoustical Society of America 98.4 (1995): 2262-2269.
- 1575
- 36 D. Kang: Target strength estimation of black porgy *Acanthopagrus schlegeli* using acoustic measurements and a scattering model. Fisheries Science 70.5 (2004): 819-828.
- 1590
- 37 H. Peña, K.G. Foote KG: Modelling the target strength of *Trachurus symmetricus murphyi* based on high-resolution swimbladder morphometry using an MRI scanner. ICES Journal of Marine Science: Journal du Conseil 65.9 (2008): 1751-1761.
- 38 G. Fairweather, A. Karageorghis, P.A. Martin: The method of fundamental solutions for scattering and radiation problems. Engineering Analysis with Boundary Elements 27.7 (2003): 759-769.
- 1595
- 39 J. Antonio, A. Tadeu, L. Godinho: A three-dimensional acoustics model using the method of fundamental solutions. Engineering Analysis with Boundary Elements 32.6 (2008): 1605
- 40 L. Godinho, P. Amado-Mendes, J. Carbajo, J. Ramis: 3D numerical modelling of acoustic horns using the method of fundamental solutions. Engineering Analysis with Boundary Elements 51 (2015): 64-73.
- 1610
- 41 E. Costa, L. Godinho, J. Santiago, A.

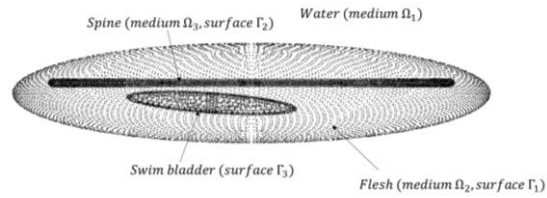
- Pereira: Prediction of acoustic wave propagation in a shallow water configuration using the Method of Fundamental Solutions. *Journal of Computational Acoustics* 20.04 (2012): 1250013.
- 1615
- 162042 L. Godinho, E. Costa, A. Pereira, J. Santiago: Some observations on the behaviour of the method of fundamental solutions in 3D acoustic problems. *International Journal of Computational Methods* 9.04 (2012): 1250049.
- 1625
- 43 K.G. Foote: Importance of the swimbladder in acoustic scattering by fish: A comparison of gadoid and mackerel target strengths. *The Journal of the Acoustical Society of America* 67.6 (1980): 2084-2089.
- 1630
- 44 T. N., Forland, H., Hobæk, E., Ona, & R. J. Korneliussen, (2014). Broad bandwidth acoustic backscattering from sandeel—measurements and finite element simulations. *ICES Journal of Marine Science: Journal du Conseil*, 71(7), 1894-1903.
- 1640
- 45 V.C. Anderson, (1950). Sound scattering from a fluid sphere. *The Journal of the Acoustical Society of America*, 22(4), 426-431.
- 1645
- 46 I.S. Prario, J.D. Gonzalez, A. Madirolas, S. Blanc: A Prolate Spheroidal Approach for Fish Target Strength Estimation: Modeling and Measurements. *Acta Acustica united with Acustica* 101.5 (2015): 928-940.
- 1650
- 47 H. Medwin, C.S. Clay: *Fundamentals of acoustical oceanography*, ed. Academic Press, Boston, 1998.
- 1655
- 48 N. Gorska, E. Ona, R. Korneliussen: Acoustic backscattering by Atlantic mackerel as being representative of fish that lack a swimbladder. *Backscattering by individual fish*, *ICES Journal of Marine Science: Journal du Conseil* 62.5 (2005): 984-995.
- 1660
- 49 R.W.G. Haslett: The back-scattering of acoustic waves in water by an obstacle II: determination of the reflectivities of solids using small specimens. *Proceedings of the Physical Society* 79.3 (1962): 559
- 1665
- 50 E. Ytteborg, G. Baeverfjord, J. Torgersen, K. Hjelde, H. Takle: Molecular pathology of vertebral deformities in hyperthermic Atlantic salmon (*Salmo salar*).
- 1670
- 1675

- BMC Physiology 10.1 (2010): 1.
- 51 J. Gu, A.M.Bakke, E.C. Valen, I. Lein, Å. Krogdahl: Bt-maize (MON810) and Non-GM Soybean Meal in Diets for Atlantic Salmon (*Salmo salar* L.) Juveniles—Impact on Survival, Growth Performance, Development, Digestive Function, and Transcriptional Expression of Intestinal Immune and Stress Responses. *PloS one* 9.6 (2014): e99932.
- 1680
- 1685
- 52 W.C. Acker: Acoustic assessment of North Pacific salmon stocks. *Rapports et Proces-Verbaux des Reunions (ICES)* 170 (1977).
- 1690
- 53 J.J. Burczynski, R.L. Johnson, H. Kreiberg, W.B. Kirchner: Acoustic estimation of dense aggregations of fish in sea pens. *Rapports et Procès-Verbaux des Réunions du Conseil International pour l'Exploration de la Mer* 189 (1990): 54-64.
- 1695
- 1700 54 E. Soliveres-González: Estimación de biomasa de peces en granjas marinas mediante ultrasonidos. Ph. D. Diss. (in Spanish) Universitat Politècnica de València, 2015.





a)



b)

Figure 1 – Illustrative sketch of the problem geometry: a) Generic representation of the idealized swimbladdered fish model. Swimbladder is approximated as a prolate spheroid and fish spine as a straight cylinder with smooth edges. X-Ray image of a salmon from [50]; b) representation of the collocation point distribution in the MFS model of the flesh, the spine the swim bladder.

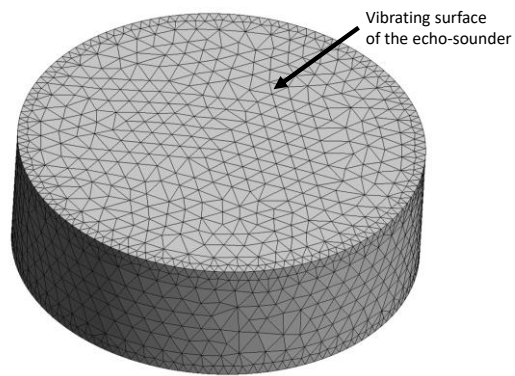


Figure 2 – Discretization of the echo-sounder's surface in small triangles.

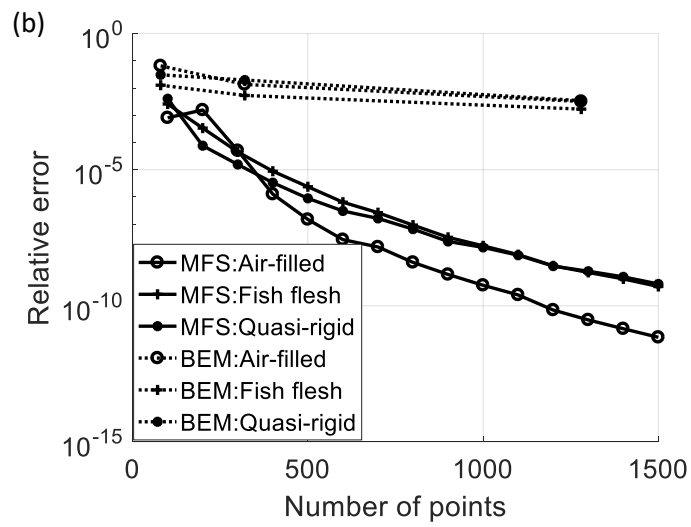
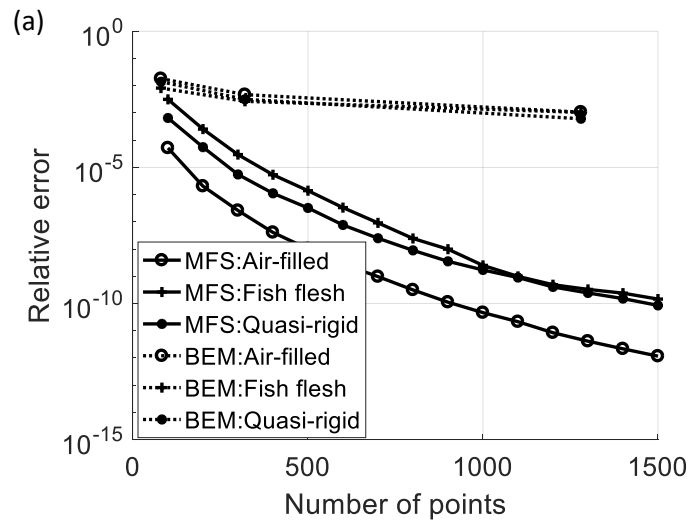
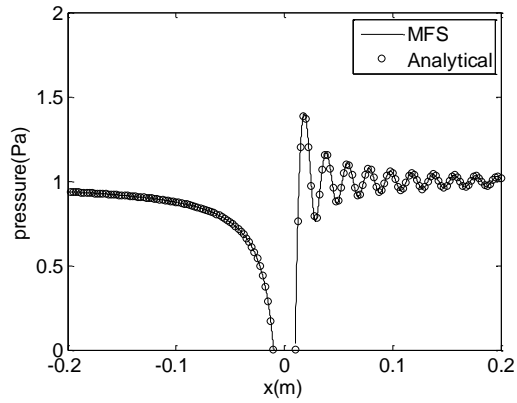
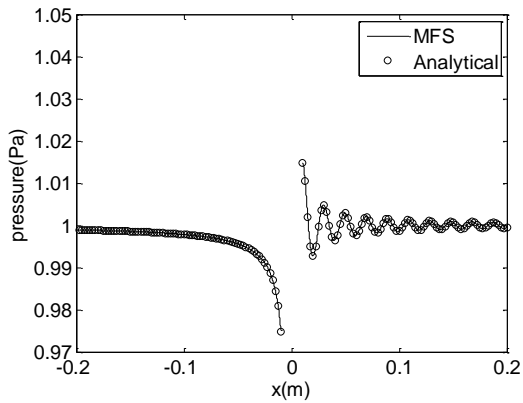
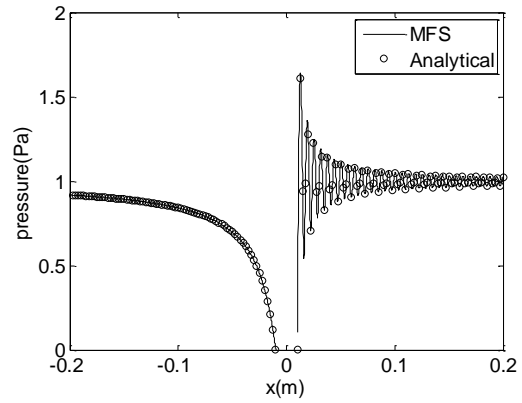


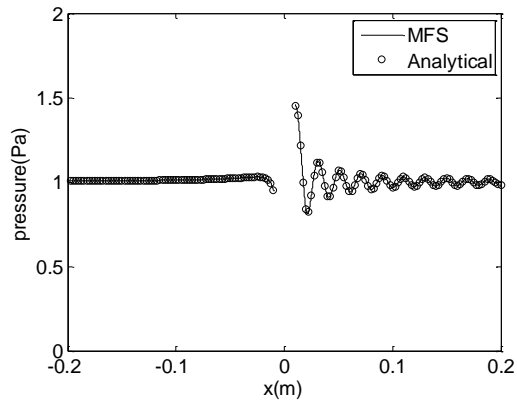
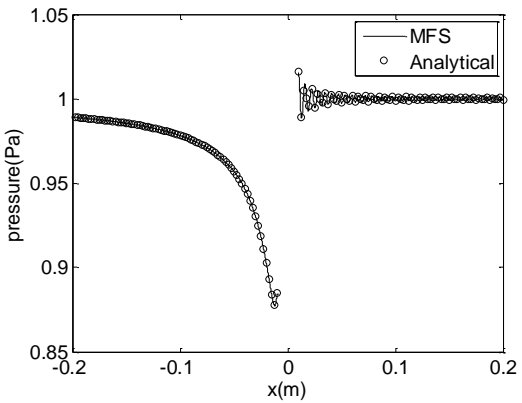
Figure 3– Relative error of the numerical calculations for the benchmark fluid-filled sphere problem, considering increasing numbers of collocation points (or elements, in the case of the BEM), for: a) 38 kHz; b) 120 kHz.



a)



b)



c)

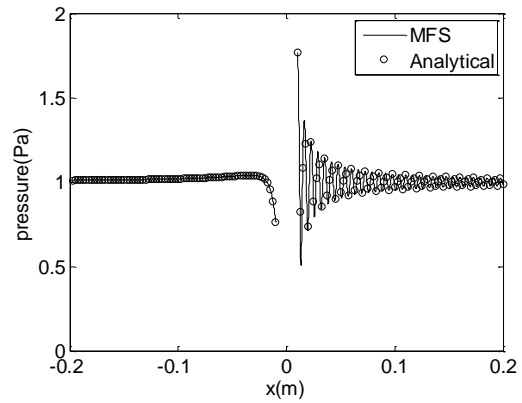


Figure 4 – Pressure along a line of receivers for the case of the fluid-filled sphere, calculated using the MFS and analytically. Left column corresponds to a frequency of 38 kHz and right column to a frequency of 120 kHz. The properties of the filling fluid are: (a) fish-flesh; (b) air; (c) quasi-rigid sphere.

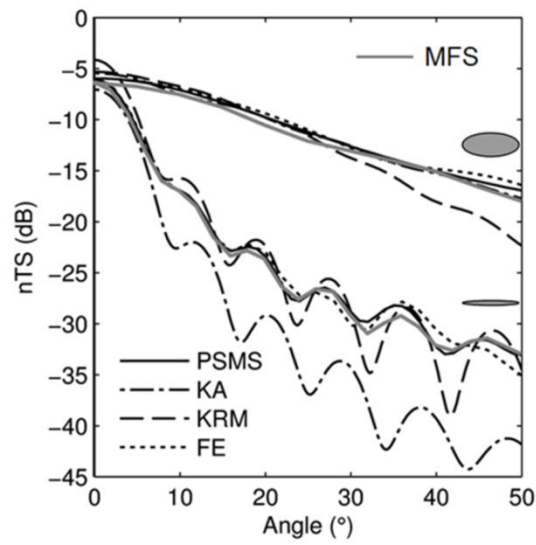
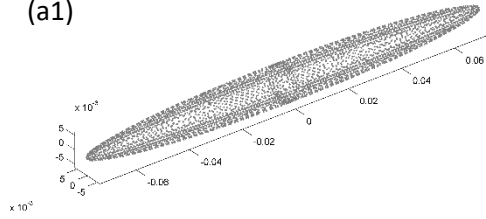
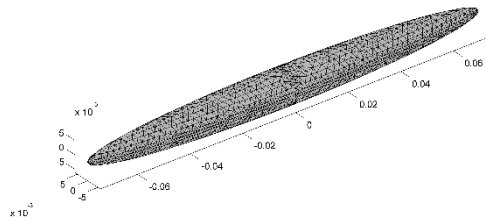


Figure 5 – Comparison of MFS method scattering results with results from PSMS, KA, KRM and FEM models from [30]. Results plot length-normalized target strength (nTS) for two prolate spheroids with  $ka=12$  and  $kb=5$  (upper lines) and  $ka=13$  and  $kb=1$  (lower lines) as a function of angle off broadside. Curves for PSMS, KA, KRM and FEM from *Figure 4* of [20].

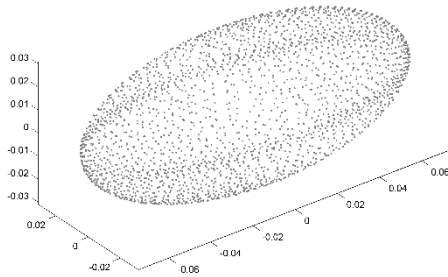
(a1)



(a2)



(b1)



(b2)

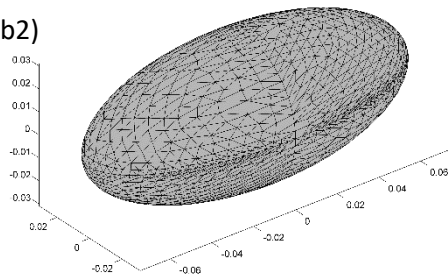


Figure 6 – Discretization of the surface of the two analysed prolate spheroids using MFS (a1 and b1) and BEM (a2 and b2). In (a), the prolate spheroid has a transverse radius of 1.24 cm, while in (b) the transverse radius is 6.18 cm.

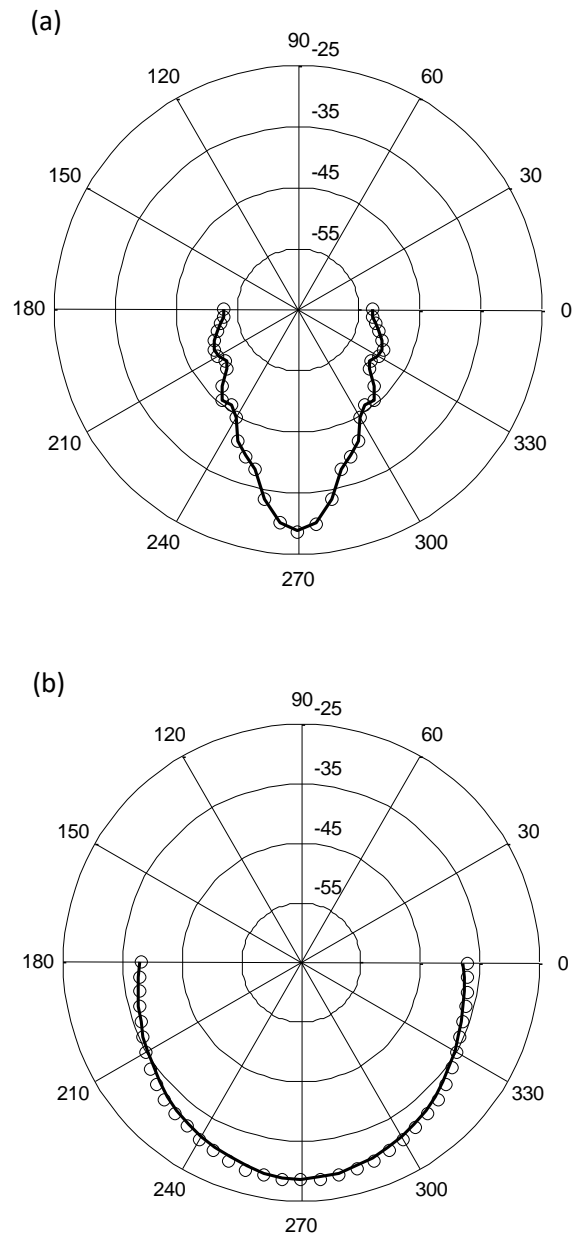
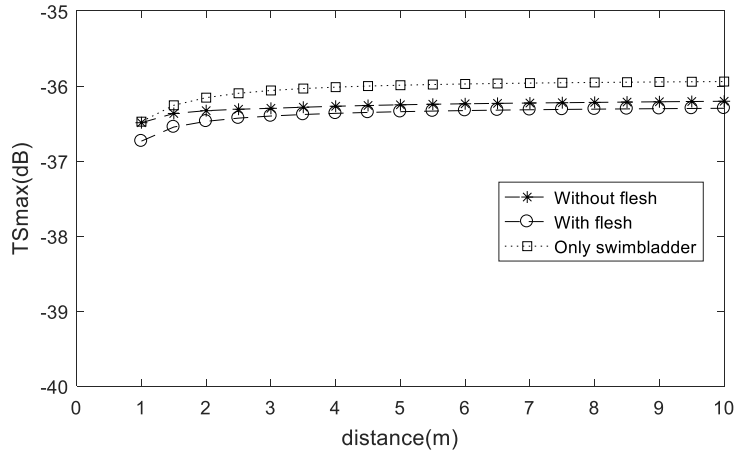
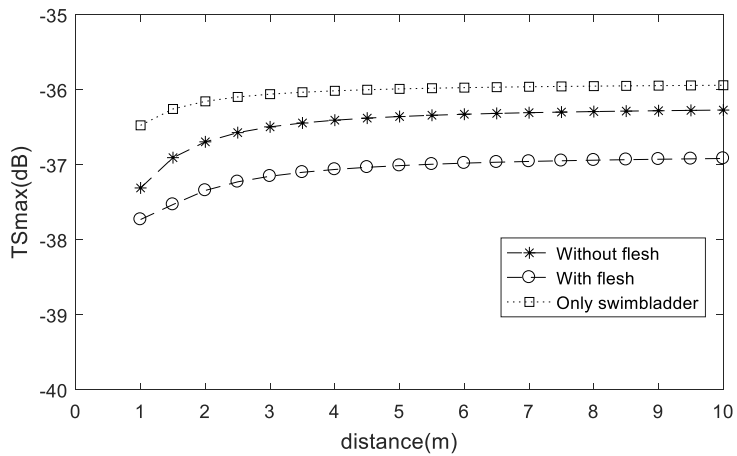


Figure 7 – Directivity plot calculated 10 m away from the spheroids, considering the MFS (full line) and the BEM (circles): a) prolate spheroid with transverse radius of 1.24 cm; b) prolate spheroid with transverse radius of 6.18 cm.



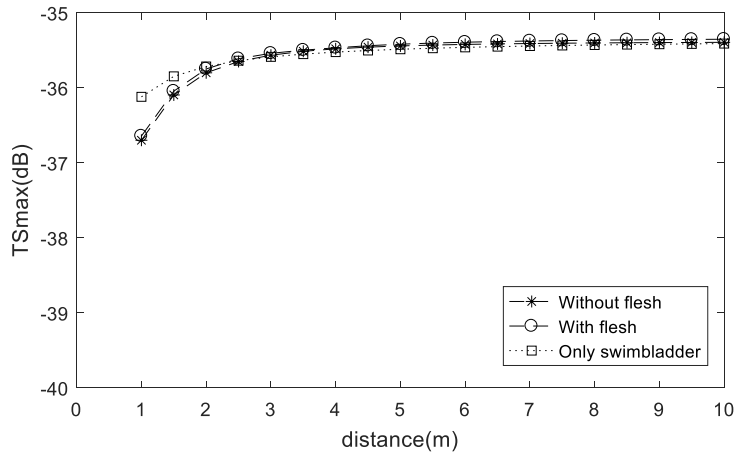
a)



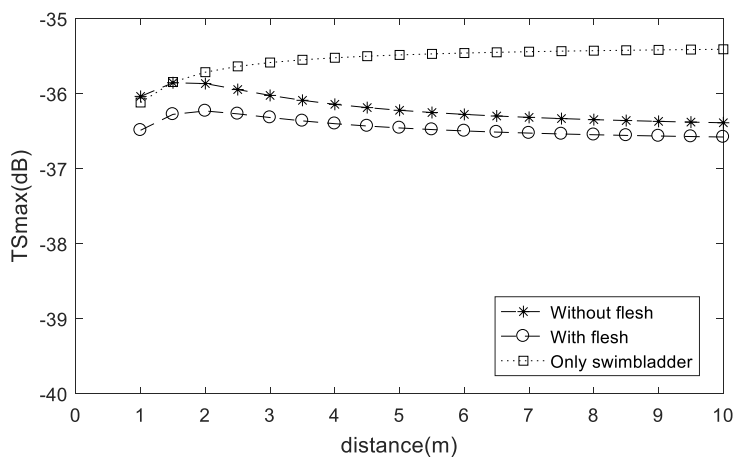
b)

Figure 8— Calculated TS at 70 kHz for ventral (a) and dorsal (b) insonification for a 18 cm fish as a function of the distance between the transducer and the fish. Three curves are represented, corresponding to the calculation considering the complete fish model including the flesh (dashed line with circle marks), just considering the spine and swim bladder (dashed line with star marks), and only accounting for the swim bladder (dotted line with square marks).





a)



b)

Figure 9. Calculated TS at 120 kHz for ventral (a) and dorsal (b) insonification for a 18 cm fish as a function of the distance between the transducer and the fish. Three curves are represented, corresponding to the calculation considering the complete fish model including the flesh (dashed line with circle marks), just considering the spine and swim bladder (dashed line with star marks), and only accounting for the swim bladder (dotted line with square marks).

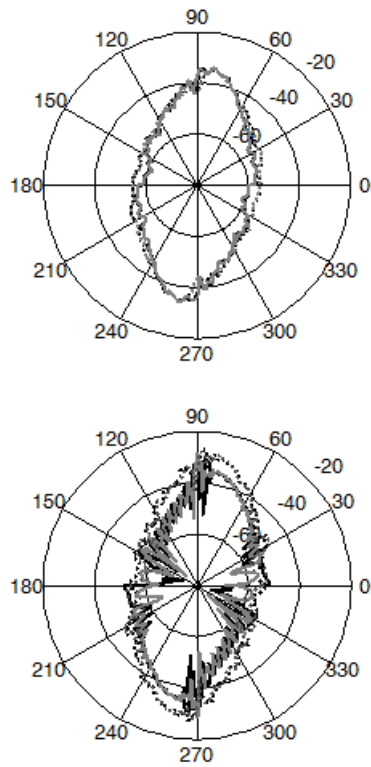


Figure 10 – Dorsal (90°) and ventral (270°) TS directivity on the x-y plane calculated at 70 kHz (dashed) and 120 kHz (continuous line) for fish length L=24 cm (upper) and L=72 cm (lower). Transducer-to-fish distance d=6 m (black line) and d=18 m (grey line).

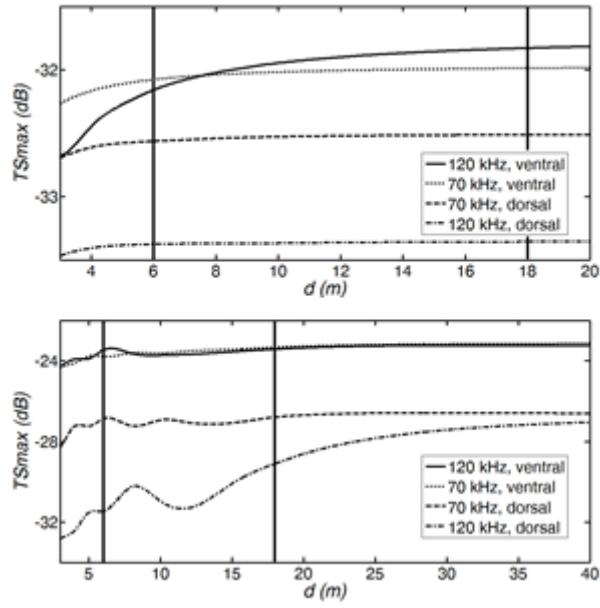


Figure 11– Evolution of  $TS_{max}$  with transducer-to-fish distance  $d$  at 70 kHz and at 120 kHz for  $L=24$  cm (upper) and  $L=72$  cm (lower). Distances are larger than the far-field distance of the transducer. Vertical lines correspond to the minimum and maximum working distances in [14].

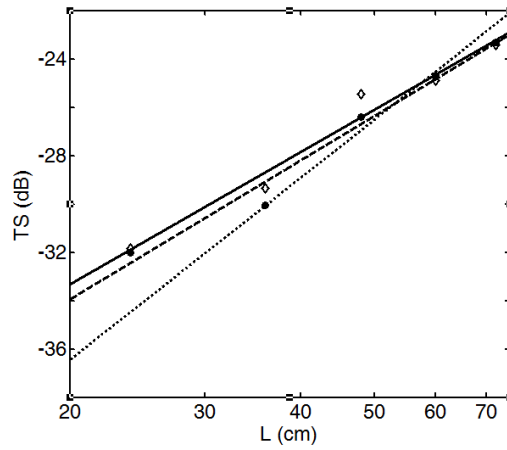


Figure 12. Regression curves for  $TS_{max}$  versus fish length considering ventral fish aspect calculated at 70 kHz (dashed line) and 120 kHz (continuous line) at  $d=18$  m corresponding to Eqs. (13) and (14), respectively. Calculated values are included as circles (70 kHz) and diamonds (120 kHz). Regression fit of mean TS-to-fish length from experimental results ventrally measured at 120 kHz in [13] are included (dotted line).